

NONLINEAR CRITERION FOR THE STABILITY OF MOLECULAR CLOUDS

RUBEN KRASNOPOLSKY AND CHARLES F. GAMMIE

Center for Theoretical Astrophysics, University of Illinois at Urbana-Champaign, Loomis Laboratory of Physics,
1110 West Green Street, Urbana, IL 61801

Received by ApJ 2004 May 28, accepted 2005 July 30, published 2005 December 20

ABSTRACT

Dynamically significant magnetic fields are routinely observed in molecular clouds, with mass-to-flux ratio $\lambda \equiv (2\pi\sqrt{G})\Sigma/B \sim 1$ (here Σ is the total column density and B is the field strength). It is widely believed that “subcritical” clouds with $\lambda < 1$ cannot collapse, based on virial arguments by Mestel and Spitzer and a linear stability analysis by Nakano and Nakamura. Here we confirm, using high resolution numerical models that begin with a strongly supersonic velocity dispersion, that this criterion is a fully nonlinear stability condition. All the high-resolution models with $\lambda \leq 0.95$ form “Spitzer sheets” but collapse no further. All models with $\lambda \geq 1.02$ collapse to the maximum numerically resolvable density. We also investigate other factors determining the collapse time for supercritical models. We show that there is a strong stochastic element in the collapse time: models that differ only in details of their initial conditions can have collapse times that vary by as much as a factor of 3. The collapse time cannot be determined from just the velocity dispersion; it depends also on its distribution. Finally, we discuss the astrophysical implications of our results.

Subject headings: star formation

1. INTRODUCTION

Molecular clouds evolve under the influence of self-gravity so as to condense part of their mass into dense cores and, ultimately, stars. The presence of magnetic fields can prevent or delay condensation. The possibility was first studied by Mestel & Spitzer (1956), who noted that the magnetic energy and the gravitational energy scale in exactly the same way with the radius R of the cloud ($\propto 1/R$) if flux freezing obtains. They argued that there was therefore a critical mass below which a cloud threaded by a particular field strength would be unable to collapse.

A more precise but less general argument was advanced by Nakano & Nakamura (1978), who studied the linear theory of a self-gravitating, isothermal, equilibrium sheet of plasma threaded by a perpendicular magnetic field. They found that magnetic fields stabilize the sheet against gravitational collapse if the mass-to-flux ratio is smaller than $1/2\pi\sqrt{G}$.

These results motivate the definition of a dimensionless mass-to-flux ratio,

$$\lambda \equiv 2\pi\sqrt{G}\frac{\Sigma}{B}, \quad (1)$$

where Σ is the column density of the sheet, and B is the magnetic field strength. The exact coefficient used to define λ depends somewhat on the geometry of the collapse. Here we have chosen the coefficient most relevant to the magnetic field geometry adopted in this paper, tending to produce thin sheets, in agreement with the expectations for magnetically supported clouds. Clouds with $\lambda > 1$ are termed *supercritical*, and clouds with $\lambda < 1$ are termed *subcritical*.

Both the Mestel & Spitzer and the Nakano & Nakamura models consider exact equilibria. Molecular clouds are far from equilibrium, however, with near-virial, highly supersonic velocity dispersion. These internal velocities must arise from strong turbulence.¹ Turbulence might change the stabil-

ity properties of the cloud, either by compressing a $\lambda < 1$ flow until it collapses, or by providing turbulent support to a cloud with $\lambda > 1$.

Many works have suggested that turbulence could provide support to star-forming clouds. Chandrasekhar & Fermi (1953) included turbulent support in their model for interstellar gaseous structures. Mestel & Spitzer (1956) pointed out that turbulence tends to decay, and that turbulence of amplitude large enough to support a cloud against self-gravity would decay especially quickly, although allowing the possibility that a strong magnetic field might perhaps allow longer lived turbulence. The supersonic linewidths observed in molecular clouds were attributed to radial motions inside the cloud instead of turbulence by Goldreich & Kwan (1974). Zuckerman & Palmer (1974) argued that if this interpretation were true for all clouds where such fluctuations are observed, the star formation rate would be too large by at least one order of magnitude. Arons & Max (1975) then suggested that the observed velocity fluctuations are due to hydromagnetic waves. By the late 1980s, this idea was widely accepted (e.g., Shu, Adams, & Lizano 1987). In the late 1990s, however, a succession of numerical experiments (Mac Low et al. 1998; Stone, Ostriker, & Gammie 1998; Gammie & Ostriker 1996) strongly suggested that the damping time of turbulence in magnetized molecular clouds is close to the dynamical time. If one accepts this, then turbulent pressure can be effective in supporting self-gravitating clouds only if it is constantly replenished, in which case the support is perhaps more readily identified with the stirring mechanism than with the turbulence itself.

Other work has tended to emphasize the role of turbulence in initiating gravitational collapse (e.g., Mac Low & Klessen 2004). Regions with a convergent velocity field will naturally tend to collapse sooner than regions with divergent velocity fields. It seems highly likely that some parts of molecular clouds have strongly convergent velocity fields; is this ever enough to overcome the stabilizing effects of the mag-

pressible equations of motion, suffer from a parametric instability with a dynamical decay rate (Sagdeev & Galeev 1969; Goldstein 1978).

¹ The most plausible alternative to turbulence, some type of weakly dissipative ordered flow, does not emerge naturally in any relevant numerical experiments that we are aware of. The mode-mode coupling is always strong. Even circularly polarized Alfvén waves, which are exact solutions to the com-

netic field? Can a subcritical cloud be induced to collapse by squeezing, or can a supercritical cloud be prevented from collapsing by the introduction of turbulence? The purpose of this paper is to investigate these questions using a simple series of numerical experiments.

The plan of the paper is as follows. In §2 we describe the experimental design, our numerical methods, and the diffusion characteristics of our code (based on the ZEUS algorithm). In §3 we describe results, including a “fiducial” run, and the influence of physical and numerical parameters on the outcome. §4 summarizes and discusses astrophysical implications.

2. DESCRIPTION OF NUMERICAL EXPERIMENTS

We will consider the simplest possible system that can manifest sub/supercritical behavior: a two-dimensional, periodic box containing a magnetized, self-gravitating, isothermal gas. Since we are interested in studying the effects of turbulence, we will introduce a velocity field in the initial conditions with statistical properties similar to those found in interstellar clouds. We will then allow the system to evolve for many dynamical times, or until it “collapses.”

Specifically, we consider a square domain in the $x - y$ plane of size $L \times L$. The z direction points out of this plane; no quantity depends on z . The initial fluid density is $\bar{\rho}$, and the sound speed, which is constant in space and time, is c_s . The initial field is $\mathbf{B} = B_x \hat{\mathbf{x}}$, where B_x is constant. The strength of the field can be characterized by $\lambda = 2\pi\sqrt{G\bar{\rho}}L/B_x$. We set the initial value of $\langle B_z \rangle = 0$, because otherwise in this z -independent geometry, asymptotically there is no collapse.

The initial velocity field is a Gaussian random field with zero divergence, constructed as in Ostriker, Gammie, & Stone (1999). The initial velocity field has a power spectrum $\langle v_k^2 \rangle \propto k^{-3}$ for $2\pi/L < k < 8(2\pi/L)$ and $\mathbf{k} \cdot \mathbf{v}_k = 0$. This power spectrum is consistent, in 2D, with Larson’s Law $v_\lambda \sim \lambda^{1/2}$, which is equivalent to an energy spectrum $E_k \sim k^{-2}$ (in 3D Larson’s Law implies $\langle v_k^2 \rangle \propto k^{-4}$). The velocity is normalized so that the kinetic energy E_K matches the desired value, and 1/3 of the kinetic energy is in motions perpendicular to the $x - y$ plane of the simulation.

2.1. Spitzer sheets and simulation units

In our experiments we will frequently find that matter flows along magnetic field lines to form sheets normal to the field. These sheets are given coherence by the self-gravity of the medium. Spitzer (1942) was the first to consider the problem of the vertical structure of an infinite, self-gravitating, isothermal sheet. Spitzer’s solution turns out to be highly useful in understanding the evolution of our simulations. Spitzer found that the equilibrium density profile of a sheet of surface density Σ is $\rho(z) = (\Sigma/2H)\text{sech}^2(z/H)$ where $H = c_s^2/(\pi G\Sigma)$. The corresponding gravitational potential and field are $\phi_S = 2c_s^2 \log(\cosh(z/H))$ and $g = -2\pi G\Sigma \tanh(z/H)$.

For any given Spitzer sheet formed during our simulation the surface density parameter Σ corresponds to $\bar{\rho}L_S$, where L_S is the extent of the region along the fieldlines that a given sheet has collected its mass from. At late times we can assume that $L_S \approx L$: most of the mass originally distributed along the fieldlines will be collected into the given sheets. This is true for the most massive sheets in the supercritical simulations, and it is seen even more clearly in the subcritical simulations, where at late times in the simulation a single large scale, stable sheet incorporates most of the mass of the system. In the following we will assume $L_S \approx L$ and $\Sigma = L\bar{\rho}$ for the Spitzer

sheets we are largely interested in — those that have collected most mass.

We nondimensionalize our models by setting $L = 1, \bar{\rho} = 1$, and $c_s = 1$. The simulation time unit is therefore L/c_s , the sound crossing time. In these units, Newton’s gravitational constant equals πn_J^2 , the Jeans length is $1/n_J$, the peak density ρ_S of an equilibrium Spitzer sheet of $L_S = L$ is $(\pi n_J)^2/2$, and its half-thickness H equals $(\pi n_J)^{-2}$. Notice that, because of the periodic boundary conditions the Spitzer sheets are slightly distorted, but as long as $H \ll 1$, the Spitzer solution will be approximately correct.

Most of the simulations presented in this paper have $n_J = 3$. This implies that the semithickness of the Spitzer sheet is 0.011, and if we are to resolve this with at least four grid zones we need $N > 360$, where the resolution of our uniform grid is N^2 . This rather stringent resolution requirement explains why we have chosen to study the problem in 2D rather than 3D.

This Spitzer-sheet model is especially useful when $\lambda \lesssim 1$ inside a largely ordered magnetic field, able to channel the flow into sheets, which later might become unstable and collapse, through accretion, collision, and merger. This sheet model, however, is not useful where $\lambda \gg 1$ and collapse is unconstrained by the field.

Simulation units can be converted to dimensional values by assuming for illustrative purposes a typical density $n_{\text{H}_2} = 10^2 \text{ cm}^{-3}$, and a typical temperature $T = 10 \text{ K}$. Then the sound speed $c_s = 0.19 \text{ km s}^{-1}$ fixes the unit of speed, and from the Jeans length $L_J = c_s(\pi/G\bar{\rho})^{1/2} = 1.9 \text{ pc}$ we obtain the unit of length $L = n_J L_J = 5.7 \text{ pc}$ for our standard value $n_J = 3$; a Spitzer sheet would then have a peak density of $n_{\text{H}_2} = 4.4 \times 10^3 \text{ cm}^{-3}$, and $H = 0.064 \text{ pc}$. The unit of mass is given by $\bar{\rho}L^3 = \bar{\rho}n_J^3 L_J^3 = 1.3 \times 10^3 M_\odot$. The unit of time is the sound crossing time $t_s = L/c_s \approx 30 \text{ Myr}$. A characteristic gravitational contraction time is $t_g = L_J/c_s \approx 10 \text{ Myr}$; free-fall collapse times are on the order of $0.3t_g \approx 3 \text{ Myr}$, depending on the geometry of the collapse.

The sound-crossing time of a Spitzer sheet is $\sim H/c_s \approx 0.3 \text{ Myr}$. From the Spitzer sheet parameters ρ_S and H it is possible to define a characteristic “Spitzer” mass $M_S = (\pi H)^2 \Sigma = c_s^4/(G^2 \Sigma) = (\pi^2 n_J^4)^{-1}$ in dimensionless units, with $\Sigma = L\bar{\rho}$. The factor of π^2 is designed to capture the mass inside half a wavelength of the shortest unstable mode of the sheet (Ledoux 1951; Elmegreen & Elmegreen 1978). For parameters typical of a molecular cloud, $M_S = 1.6 M_\odot$, which is a suggestive result. This may be compared with the thermal Jeans mass $M_J = \bar{\rho}L_J^3 = \pi^{3/2}c_s^3/G^{3/2}\bar{\rho}^{1/2} = n_J^{-3}$ in dimensionless units, with a typical value of $M_J = 49(T/10 \text{ K})^{3/2}(n_{\text{H}_2}/10 \text{ cm}^{-3})^{-1/2} M_\odot$.

2.2. Ambipolar diffusion

Our simulation utilizes the ideal MHD equations, which have some well-known limitations. Ambipolar diffusion is expected to become relevant (Kulsrud & Pearce 1969) at length-scales smaller than the damping length for Alfvén waves, $L_{\text{AD}} \sim v_A t_{ni}$, where $v_A = B/\sqrt{4\pi\bar{\rho}}$, and $t_{ni} = 1/(Kn_i)$, with $K \approx 1.9 \times 10^{-9} \text{ cm}^3 \text{ s}^{-1}$ (Draine, Roberge, & Dalgarno 1983). The number density of ions n_i may depend strongly on environmental factors, such as the UV illumination and its attenuation by the cloud material (Ciolek & Mouschovias 1995; McKee 1989); it also depends on chemical properties, such as the metal abundance in the gas phase. For our fiducial mean density $\bar{\rho}$, a representative value could be $n_i \sim 2 \times 10^{-4} \text{ cm}^{-3}$,

largely limited by an assumed metal abundance $x_M \approx 10^{-6}$. For the typical peak density of a Spitzer sheet ρ_S in our conditions, $n_i \sim 6 \times 10^{-4} \text{ cm}^{-3}$ for cosmic-ray dominated ionization, and about ten times larger for regions of the cloud that are moderately well UV-illuminated.

The ambipolar diffusion lengthscale L_{AD} can now be compared with the size L of the computational volume, giving an estimate of the scale at which ideal MHD stops being a complete dynamical description of the flow. For our mean density profile, we find that this lengthscale is $L_{AD} \sim L/35$, much larger than our typical grid spacing $L/512$, and comparable to our typical sheet thickness $2H = L/45$. However, ideal MHD is still a good description of the most important portions of this study; the regions where mass is collected to form dense sheets. For $\rho = \rho_S$, the lengthscales are $L_{AD} \sim L/700$ for a UV-dark region, and $L_{AD} \sim L/7000$ for the more illuminated case. The decrease of v_A with density has contributed to this effect, together with the larger n_i .

We keep in mind, however, that densities and ionization rates vary widely inside clouds, and so the ambipolar diffusion lengthscales and timescales may vary widely. Turbulent conditions inside the flow are also expected to increase the importance of ambipolar diffusion, even at larger lengthscales, especially near sharp velocity and magnetic gradients.

2.3. Stopping criterion

We must fix some criterion for stopping the numerical integration; when the density in any zone equals or exceeds the largest allowed by the Truelove numerical stability condition (Truelove et al. 1997) the run is terminated and classified as having collapsed. The Truelove condition requires that the local Jeans length be resolved by some algorithm-dependent number N_T of grid zones, typically about 4. This requirement sets a maximum resolvable density of $\rho_T = (N/n_i N_T)^2 = 1820(N/512)^2$ for $n_i = 3$ on our uniform grid of N^2 zones. We have found that further integration of Truelove-unstable models results in large local fluctuations in the density, which can produce ‘‘explosions’’ that corrupt the entire computational domain. Runs that reach $t = 2$ without violating the Truelove condition are classified as stable.

We have experimented with other collapse detection schemes, because the Truelove criterion has the deficiency that it is resolution dependent. In the Tables described below we report not only the time t_T at which the Truelove condition is violated, but also the time t_{10} when 1% of the mass exceeds 10 times the Spitzer density ρ_S . These times are typically close to each other, and both can be considered as measures of the onset of gravitational instability. The time t_{10} has the advantage of not depending explicitly on numerical resolution, but it can be fooled into producing misleadingly short collapse times by strong density fluctuations, particularly when the turbulent kinetic energy is large.

2.4. Numerical methods and tests

Our simulations are run on a fixed 2D Cartesian grid, using the ZEUS algorithm (Stone & Norman 1992a,b) as implemented for instance in Ostriker, Gammie, & Stone (1999). ZEUS is a numerical algorithm to evolve ideal (non-resistive, non-viscous) non-relativistic MHD flows. It is operator-split, representing the fields on a (possibly moving) Eulerian staggered mesh. The magnetic field evolution uses constrained transport (Evans & Hawley 1988) which guarantees that $\nabla \cdot \mathbf{B} = 0$ to machine precision, combined with the method

of characteristics (Hawley & Stone 1995), which ensures accurate propagation of Alfvén waves. ZEUS is explicit in time, and so the timestep Δt is limited by the Courant conditions. In our problem, usually the most stringent has been $\Delta t < \Delta x/v_A$, where $v_A = B/\sqrt{4\pi\rho}$ can take very large values in density-depleted regions. A numerical density floor, ρ_{floor} , has been set to limit density depletion, preventing Δt from becoming too small; we have directly tested that this tiny non-conservation of mass by the code does not alter the simulation results regarding collapse in any way. The Poisson equation, needed to describe self-gravity, is solved by Fourier transform methods, using the FFTW code (Frigo & Johnson 2005).

Any Eulerian scheme will cause some diffusion of the magnetic field with respect to the mass. It is crucial for our experiment that this nonconservation of λ be as small as possible. The numerical diffusivity of ZEUS is difficult to estimate because, unlike a physical resistivity, it is flow dependent. An empirical approach is therefore required.

We have studied conservation of λ using two distinct methods. In the first method we initialize a non-self-gravitating box using the same initial data as in our main experiments, as described above. We evolve the computation to $t = 0.5$ and then damp the velocity field exponentially (with timescale $t_{\text{damp}} = 0.05$) until $t = 10$. If there were no λ diffusion the box would return to a uniform density, uniform field state. Diffusion changes λ , so the final state consists of a unidirectional magnetic field with density and field strength varying only perpendicular to the field, from which λ can be easily measured.

In the second method we initialize a non-self-gravitating box using the same initial data as in our main experiments, but we evolve the computation only to $t = 0.5$. We then sample 80 field lines chosen to lie at equal intervals of the vertical component of the vector potential (equivalent to lines equally spaced in magnetic flux). We then integrate $\rho / (B_x^2 + B_y^2)^{1/2}$ along the field line in the $x - y$ plane,² using linear interpolation to determine ρ and \mathbf{B} at each position, which immediately yields λ .

These two methods give nearly identical results. We therefore adopt the second method exclusively, since it can be used to probe existing numerical data without any additional, expensive evolution.

One possible figure of merit for the diffusion in λ is $\sigma_\lambda / \lambda_0$, where σ_λ is the dispersion in sampled values of λ at the final instant of the simulation, and λ_0 is the nominal initial value (which we call simply λ outside of this subsection). Tables 1 and 2 show $\sigma_\lambda / \lambda_0$ as a function of resolution and of time during a single simulation, respectively. The run shown in Table 2 has a resolution of 512^2 . The key points here are that $\sigma_\lambda / \lambda_0$ decreases as resolution increases, and that in every case $\sigma_\lambda / \lambda_0$ is about 10% or less, which suggests that we should be able to measure the critical value of λ to similar accuracy.

Evidently $\sigma_\lambda / \lambda_0$ is converging, but as $\approx N^{-1/2}$ rather than the expected N^{-1} . This may be because of the existence of unresolved regions in the flow where most of the diffusion occurs, or it may be the result of irreducible ‘‘turbulent’’ diffusion that is present independent of the magnitude of the effective numerical diffusion. The numerical diffusion is correlated with the amplitude of turbulence. According to Table 2,

² This is equivalent to integrating $\rho / (B_x^2 + B_y^2 + B_z^2)^{1/2}$ along the 3D field-line.

TABLE 1
MASS-TO-FLUX DIFFUSION IN ZEUS, AS A
FUNCTION OF NUMERICAL RESOLUTION

N	t	σ_λ/λ_0	λ_{\max}/λ_0	λ_{\min}/λ_0
400	0.1	9.0 %	1.26	0.78
512	0.1	8.6 %	1.31	0.78
1024	0.1	6.1 %	1.30	0.87
2048	0.1	4.4 %	1.10	0.86
512	0.2	8.3 %	1.20	0.79
2048	0.2	4.7 %	1.12	0.85

TABLE 2
MASS-TO-FLUX DIFFUSION IN ZEUS, AS A
FUNCTION OF TIME

t	σ_λ/λ_0	λ_{\max}/λ_0	λ_{\min}/λ_0	$E_K(t)$
0	0 %	1	1	50
0.01	0.2%	1.01	0.99	37
0.02	0.9%	1.02	0.97	25
0.03	2.1%	1.05	0.92	18
0.04	3.6%	1.10	0.90	15
0.05	6.4%	1.18	0.84	16
0.06	8.0%	1.32	0.74	19
0.1	8.6%	1.31	0.78	17
0.2	8.3%	1.20	0.79	11
0.3	9.6%	1.20	0.74	8.5
0.34	11.1%	1.21	0.71	5.5

much of the diffusion occurs very early in the run, when the rms velocity is large.

Another possible figure of merit is the total variation in λ , that is, $|\lambda_{\max} - \lambda_{\min}|/(2\lambda_0)$, measuring the possible existence of localized diffusion events in addition to the overall diffusivity of the code. We find in Tables 1 and 2 that this quantity is typically of the size $\sim 2.4\sigma_\lambda$, expected in the mean for the half-range of a sample of 80 elements randomly taken from a Gaussian distribution. However, the distribution of values of λ might not always be Gaussian, because localized numerical diffusion could be important for some fieldlines. In our tables, this may be happening when λ_{\max} reaches values as large as $1.3\lambda_0$, even at the relatively high resolution of $N = 1024$. The larger total variation of λ observed in those simulations suggests a possible risk of masking the subcritical nature of some models.³ However, we also find that the total variation of λ starts to drop at the even higher resolution of $N = 2048$; numerical resolution seems apparently able to reduce also this more local measure of the diffusivity of the numerical code.

It is worth noting that ambipolar diffusion in nature is likely strong enough to dominate the diffusion measured here. For our nominal cloud parameters, we have seen in §2.2 that the damping length of Alfvén waves is of the same order as the expected thickness of an equilibrium sheet. Thus our models may misrepresent the situation in nature by tying the fluid too closely to the magnetic field. The combination of ambipolar diffusion and turbulence (which can drive sharp features for the ambipolar diffusion to act on) may be a potent driver of variations in mass-to-flux ratio in Galactic molecular clouds.

3. RESULTS

3.1. Fiducial run

³ As a possible example of this effect, in Table 5 one model collapses despite having $\lambda_0 = 0.9$; also the very low resolution models with $N = 128$ that collapse for $\lambda_0 = 0.744$.

As a guide to the dynamics of our numerical experiments, we will first describe a “fiducial” run, whose behavior is in a sense typical of the other experiments. This run is supercritical, with $\lambda = 1.5$, initial $E_K = 50$ (equivalent to an rms Mach number of 10), $n_I = 3$, and $N = 512$. The panels of Figures 1 and 2 show how condensation proceeds. At first, small density concentrations form due to both ram pressure associated with the supersonic velocity fluctuations in the initial conditions and fluctuations in the magnetic pressure. These later coalesce into larger clumps, typically oriented perpendicular to the magnetic field.⁴ We have seen that these clumps develop into fully stable Spitzer sheets in the simulations of subcritical clouds; here they can be considered also as approximate Spitzer sheets, which later come unstable, as the peak density of these sheets grows. This density growth takes place when the clumps merge or collide, and when matter accretes from outside the sheet. The largest density of these clumps increases as shown in Fig. 3; slowly at the beginning, but very steeply close to the end of the run. The energies, on the other hand, vary smoothly in time (Fig. 4), and are not a good predictor of the time required for instability.

At a time $t_{10} = 0.325$, the fraction of matter denser than 10 times the nominal Spitzer density includes more than 1% of the mass $\rho_{1\%}(t) > 10\rho_S$. Not long afterwards, at a time $t_T = 0.341$ (soon after the last panel in Fig. 1) the peak density of the simulation box exceeds the Truelove limit, forcing an end to the run. We conclude that the initial state of this fiducial run represents an unstable cloud, able to produce dense cores. These two times are much larger than the linear e-folding time found in Nakano (1988) (≈ 0.035 for $\lambda = 1.5$); collecting matter into the unstable structures takes a longer time than the instability process, linear or nonlinear, and dominates the total time necessary to achieve instability in the mildly supercritical clouds. Using our nominal conversion factors from simulation to physical units, $t_{10} = 9.8$ Myr.

3.2. The nonlinear stability criterion

To discover how precisely the criticality condition was obeyed in the numerical experiments, we considered a series of runs with $E_K = 50$ and $E_K = 10$ while gradually varying λ . Table 3 lists the collapse times for each of these runs. Evidently the criticality condition is very nearly obeyed in the numerical evolutions, and there is no evidence of collapse induced by compression. Indeed, given the diffusion of λ measured in §2, it is remarkable (from a numerical standpoint) that we are able to reproduce the condition so accurately. Some sense of the “error bars” can be obtained by noticing that the $\lambda = 1$ model with $E_K = 50$ does collapse, while the $\lambda = 1.02$ model with $E_K = 10$ does not. This suggests that the Nakano & Nakamura condition is the true nonlinear stability condition.

Tables 4 and 5 show a clear trend to make the simulations shorter lived as λ increases. This trend is expected from the already observed stability criterion.⁵ Models with $\lambda \approx 1$ can be quite long lived; the $\lambda = 1$, $E_K = 50$ model persists until $t = 0.756$, or about 23 Myr for our nominal cloud parameters.

The run with $\lambda = 1.05$ and $E_K = 10$ has been done twice, with different values of the numerical density floor; the col-

⁴ Clumps do not tend to orient perpendicular to the field in our three-dimensional models (Gammie et al. 2003). Those runs had a resolution of 256^3 , however, and the supercritical runs did not have λ as close to 1 as the models considered here.

⁵ The most strongly supercritical models ($\lambda \gtrsim 10$) collapse very quickly, in around one free-fall time.

lapse times are identical up to reasonable precision. This allows us to trust the runs using the larger density floor, which are much more convenient because it allows a larger timestep, largely controlled by the maximum value of the Alfvén speed $B/\sqrt{4\pi\rho}$ on the grid. From here on, we will not report the values of this purely numerical parameter in these simulations.

3.3. Influence of the turbulence energy and distribution

We have also investigated the effect of the amplitude and structure of the initial velocity field. Table 4 shows the results from a series of runs with $n_J = 3$ and $N = 512$. The column marked “Seed” is the seed used to initiate the random number generator used to generate the initial velocity field. Runs with the same seed but different initial kinetic energies have velocity fields that are linearly proportional to each other.

The first series of runs with seed = 1 show a monotonic increase in the lifetime of the cloud with kinetic energy, consistent with results reported elsewhere (Gammie & Ostriker 1996; Ostriker, Gammie, & Stone 1999). The effect is weak at low energies but more pronounced once $E_K > 50$.

An even larger effect is obtained by changing the structure of the initial velocity field, i.e. by changing the seed. We find that models that differ only in the initial seed can have collapse times that vary by up to a factor of 3.

To further explore this effect, we performed a series of runs, choosing sixty different values of the random seed used to set up the shape of the initial velocity distribution. In this series, we have fixed $\lambda = 1.5$, $E_K = 50$, $N = 512$, and $n_J=3$. The results can be seen in Figure 5, showing a wide distribution of collapse times. The total range of this sample goes from $t_T = 0.228$ to $t_T = 0.667$, equal to ~ 7 to 20 Myr for the typical cloud parameters used in §2. The mean time is $\langle t_T \rangle = 0.368$ (~ 11 Myr); the median is located at $t_T = 0.355$, and the peak near $t_T = 0.3$, showing a moderate asymmetry. This asymmetry is more pronounced in the tails: $t_T < 0.2$ is not observed in the sample; while a few values of $t_T > 0.5$ (at a similar distance from the median but in the opposite direction) are present in the distribution, corresponding to clouds lasting between ~ 15 and 20 Myr before collapse, much longer than the mean lifetime value.

This stochastic variation in cloud lifetime doubtless has a counterpart in nature. The origin of this variability is clear: almost all velocity variations occur at the largest scales, and are driven by just a few Fourier modes. If these modes happen to have the right amplitude and phase then collapse is hastened. If they are unfavorable, then collapse can be delayed by as much as 12 Myr for our nominal cloud parameters.

3.4. Influence of numerical parameters

The influence of the density floor ρ_{floor} has already been shown in §3.2 to be fully negligible, provided this floor is not unreasonably large.

Numerical resolution, on the other hand, can be quite relevant. Any serious simulation of condensation in a nearly critical cloud must be able to resolve the half-thickness H of a Spitzer sheet, requiring at the very minimum $N > 1/H = (\pi n_J)^2$. For our fiducial choice of $n_J=3$, this requires a minimum of $N > 89$, and more reasonably $N > 200$; any simulation run at smaller resolution would not be exploring the most basic physics of mass condensation. However, this requirement does not seem to take care of all the effects of numerical resolution.

Table 5 lists simulations where we have varied the number N of active zones in the grid on each direction. There is

TABLE 3
MODELS WITH λ CLOSE TO 1

λ	E_K	ρ_{floor}	t_{10}	t_T
1.1	50	10^{-6}	0.304	0.376
1.05	50	10^{-4}	0.387	0.500
1.0	50	10^{-4}	0.497	0.756
0.95	50	10^{-4}	> 2	> 2
0.9	50	10^{-4}	> 2	> 2
1.1	10	10^{-6}	0.314	0.367
1.05	10	10^{-6}	0.702	0.741
1.05	10	10^{-4}	0.702	0.741
1.02	10	10^{-4}	> 2	> 2
1.0	10	10^{-4}	> 2	> 2
1.0	10	10^{-6}	> 2	> 2
0.9	10	10^{-6}	> 2	> 2

NOTE. — Parameters kept fixed in these runs: $n_J = 3$, $N = 512$, random seed = 2.

TABLE 4
SUPERCRITICAL AND
SUBCRITICAL MODELS

λ	E_K	Seed	t_{10}	t_T
1.5	100	1	0.601	0.615
1.5	70	1	0.521	0.533
1.5	50	1	0.325	0.341
1.5	20	1	0.260	0.270
1.5	10	1	0.250	0.257
1.5	1	1	0.259	0.269
1.5	50	2	0.126	0.211
1.5	20	2	0.193	0.200
1.5	10	2	0.233	0.244
1.5	50	3	0.510	0.537
1.5	20	3	0.346	0.360
1.5	10	3	0.299	0.310
1.5	1	3	0.314	0.324
1.2	100	1	0.715	0.744
1.2	50	1	0.376	0.400
1.1	100	1	0.787	0.910
1.1	50	1	0.377	0.534
1.1	100	2	0.314	0.372
1.1	50	2	0.304	0.376
1.1	10	2	0.314	0.367
1.1	50	3	0.735	0.746
0.8	100	2	0.216	> 2
0.8	10	2	> 2	> 2
0.8	10	3	0.664	> 2
0.8	1	3	> 2	> 2

NOTE. — Parameters kept fixed in these runs: $n_J = 3$, $N = 512$.

a clear tendency for the more resolved simulations to delay t_T . This was in part expected, as the Truelove limit density $\rho_T = (N/n_J N_T)^2$ depends steeply on N . This is not, however, the main reason for the observed trend. Peak densities grow very quickly in the neighborhood of the condensation time, almost nullifying in most cases the influence of the exact magnitude of ρ_T on the value of t_T . The quantity t_{10} is expected to be less directly dependent on resolution, having a definition where N does not appear; it still shows some dependence on resolution, closely correlated to the dependence shown by t_T , and probably due to details of the dynamics being more revealed at higher resolutions and to reduced numerical diffusion.

Most of our simulations were performed at $N = 512$. For comparison purposes, a simulation run with the same initial conditions as the fiducial run, but with $N = 2048$, has $t_T =$

TABLE 5
SUPERCRITICAL AND SUBCRITICAL
MODELS RUN AT DIFFERENT NUMERICAL
RESOLUTIONS

λ	E_K	Seed	N	t_{10}	t_T
∞	50	1	512	0.068	0.077
∞	50	1	1024	0.071	0.083
1000	50	1	512	0.068	0.077
10	50	1	512	0.112	0.124
1.5	50	1	256	0.283	0.283
1.5	50	1	400	0.305	0.312
1.5	50	1	512	0.325	0.341
1.5	50	1	1024	0.409	0.434
1.5	50	1	1536	0.429	0.453
1.5	50	1	2048	0.445	0.481
1.5	20	1	512	0.260	0.270
1.5	20	1	1024	0.263	0.283
1.5	10	1	512	0.250	0.257
1.5	10	1	1024	0.253	0.273
1.2	50	1	256	0.319	0.319
1.2	50	1	512	0.376	0.400
1.2	50	1	1024	0.504	0.523
1.1	100	2	512	0.314	0.372
1.1	100	2	1024	0.337	0.738
0.9	100	2	512	0.079	0.351
0.9	100	2	576	0.079	> 2
0.9	100	1	512	> 2	> 2
0.85	100	2	512	0.075	> 2
0.8	100	2	512	0.216	> 2
0.8	50	1	256	> 2	> 2
0.7	100	2	512	0.435	> 2
0.6	50	1	256	> 2	> 2

NOTE. — Parameter kept fixed in these runs: $n_J = 3$.

TABLE 6
MODELS WITH DIFFERENT
VALUES OF n_J .

n_J	λ	Seed	N	t_T
2.5	1.2	1	512	0.87
	1.2	2	256	0.44
	1.2	3	256	0.83
	1.1	1	256	0.75
	1.1	2	256	0.48
	1.1	3	256	0.82
	1.1	3	512	1.21
	1.1	4	256	0.49
	0.9	3	512	> 2
	2.0	1.2	1	256
1.2		1	512	1.87
1.2		2	256	1.00
1.2		3	256	1.50
1.15		2	256	1.33
1.15		3	256	> 2
1.1		1	256	> 2
1.1		1	512	> 2
1.1		2	256	9.77
1.1		2	512	> 2
1.1		3	256	> 2
1.1		3	512	> 2
1.1		4	256	> 2
0.9		3	512	> 2

NOTE. — Parameter kept fixed in these runs: $E_K = 50$.

0.445 and $t_{10} = 0.481$, noticeably larger, but not enough to change the qualitative conclusions.

One of the subcritical models with $\lambda = 0.9$ and $N = 512$ (Table 5) is remarkable because the run presents an unexpected collapse at $t_T = 0.351$. However, the same table shows

that either changing the numerical seed, or a moderate increase in numerical resolution is enough to suppress this unusual behavior; also a small change in λ can suppress this apparently purely artificial collapse.

We have also run a few comparison simulations at $N = 128$. This resolution is insufficient to represent equilibrium Spitzer sheets, and indeed the models collapse even for $\lambda = 0.744$. This is due to the excessively low resolution: it is just enough to accommodate one sheet semithickness per grid zone, and, through the Truelove stability criterion, it allows only a narrow density range, limited by $\rho_T = (N/n_J N_T)^2 = 114\bar{\rho} = 2.6\rho_S$, insufficient to accommodate an eventual moderately large oscillation in the density ρ_S of the equilibrium sheets formed in subcritical simulations.

In another series of tests, we started the simulations from an equilibrium sheet, and let it evolve in the presence of a very small perturbation. For the values $\lambda = 1.5$ and $\lambda = 2$, the perturbation grows linearly with e -folding times equal to 0.036 ± 0.001 and 0.027 ± 0.001 , quite comparable to the values predicted by the linear theory, 0.035 and 0.025, known from Nakano (1988) to a precision of 5%. For values of $\lambda < 1$, the simulations have remained stable up to a time $t \approx 4$ during a few linear test runs performed at $\lambda = 0.9$ at various resolutions.

3.5. Influence of n_J

We have performed a small set of simulations exploring the influence of n_J on the instability criterion found (Table 6). For $n_J = 3$, we had found instability for $\lambda > 1.05$; for $n_J = 2.5$, the numerical requirement is no more stringent than $\lambda > 1.1$; however, for $n_J = 2.0$, the numerical requirement for instability becomes $\lambda > 1.15$. A weak dependence of the numerical criterion on n_J had already been predicted by Nakano (1988) in the linear regime. Linearly unstable modes have a minimum critical wavelength; if we require that this wavelength must fit inside the computational box size L , we find that the instability criterion will be approximately⁶

$$\lambda > [1 - 2/(\pi n_J^2)]^{-1}, \quad (2)$$

which for small values of n_J can be more stringent than the infinite disk value $\lambda > 1$. The results in Table 6 are consistent with Eq. 2. Nakano (1988) presents for the case of a finite disk a still more stringent criterion for linear instability, $\lambda > [1 - 4/(\pi n_J^2)]^{-1}$, based on the assumption that *two* critical wavelengths should fit inside the computational box. Our slightly larger unstable range might be related to the geometric difference between a finite disk and our periodic boundary conditions. Spitzer sheets pull in magnetic field lines during their formation and contraction (Fig. 2); this may also allow collapse at smaller wavelengths than expected in a purely linear theory.

4. CONCLUSIONS

Our simulations confirm that the single most important element in determining the long term gravitational stability of turbulent magnetized clouds is indeed the mass-to-flux ratio, dividing supercritical from subcritical clouds. The relevant coefficient is that corresponding to a sheet geometry, as derived by Nakano & Nakamura (1978).

⁶ Following Nakano (1988), certain integrals involving generalized Riemann zeta functions have been replaced by simpler expressions. These approximations are excellent inside our range of interest $n_J \geq 2$.

Turbulent energy has comparatively little influence on the presence or absence of stability, up to Mach numbers ~ 10 . Subcritical clouds will develop density concentrations due to this turbulence, but under an ideal MHD regime, the consequent increase in magnetic pressure prevents further collapse. However, total turbulent energy has some influence on the lifetime of supercritical clouds, especially as the Mach number becomes large enough (of the order of ~ 7 in these simulations).

More interesting is the fact that turbulence introduces a stochastic element. The collapse time cannot be predicted with certainty from physical parameters such as the mass and field in the cloud, and the typical energy of the turbulence motions, because the random distributions of velocity and density can change the lifetime by some factor, seen to be of the order of 3 in one large sample. The resulting distribution of lifetimes has an asymmetric tail of unusually long-lived clouds. We suggest that the existence of such a tail may introduce a bias in the observed samples of star-forming clouds. Most star formation will take place in the more frequent, shorter lived clouds, while observations of clouds will tend to focus on the fewer longer lived ones.

We have seen that the numerical resolution requirements needed to study cloud collapse are very stringent, and we expect they will be even more stringent in 3D. There is a necessity of resolving the possible equilibrium structures, such as the Spitzer sheets, which we have seen fully formed in the subcritical clouds, and partially formed during the run-up to instability of the mildly supercritical ones. The thickness of these sheets scale with the number n_J of Jeans lengths as n_J^{-2} . Accommodating a large number n_J of Jeans lengths inside the computational volume will therefore be numerically challenging. Increasing n_J by only a factor of 2 requires increasing the space resolution by a factor of 4. Unless adaptive mesh refinement (AMR) is used, this requires increasing the simulation runtime by factors on the order of $64 = 4^3$ in 2D, and $256 = 4^4$ in 3D. We anticipate that AMR will be used in many of the successful simulations of core formation in the future.

Numerical stability, through the Truelove condition, sets a maximum density that can be accommodated at a given spatial resolution. Shocks in strongly turbulent flows have large compression ratios, sometimes requiring increasing resolution in order to distinguish a transient density increase due to a shock from an authentically unstable accumulation of mass able to form a collapsed object.

We have seen that artificially enforcing numerical density floors, even relatively large ones, on the order of 10^{-4} times the background density, had almost no influence in the evolution of the collapse. This result is again not surprising, because wide regions of small density have little influence on the dense, self-gravitating regions that undergo collapse. Density floors can significantly speed up ideal MHD simulations, whose Courant timestep is often limited by large Alfvén

speeds $B/\sqrt{4\pi\rho}$ in the least dense regions.

This work is limited due to the periodic boundary conditions. We believe this may have favored the collection of clumps into larger clumps until the instability can take place. Some simulations occasionally show fast-moving clumps flowing past each other, and later merging once one of them returns through the other side of the periodic computational volume. The periodic boundary conditions make it plausible that sooner or later, most of the mass in a given fieldline will collect into a single clump, which then can undergo instability if its mass is even slightly supercritical. In real clouds with ordered magnetic fields, clumps inside the same fieldline but moving in opposite directions are not expected to merge; however, it is improbable this will apply to all of the fieldlines and so we expect that the instability will still take place in a similar form, albeit with an additional stochastic factor in the cloud lifetime.

Two-dimensionality is also a limitation of this work. It has strongly limited the topological possibilities for the fieldlines; it is conceivable that the consequent limitations in motion have favored the collection of mass into massive sheets and other structures. Observations (e.g., Goodman et al. 1990; Crutcher 2004), and 3D simulations and studies (e.g., Basu 2000; Gammie et al. 2003) indeed indicate that sheets aligned perpendicular to the magnetic field are not always the preferred possibility for the long term development of clouds. More variety of clump shapes is expected in a 3D study. The larger variety in motions allowed by a 3D magnetic field is expected to enhance the already observed stochastic effects, and perhaps might also delay mass collection into potentially unstable structures. However, even in 3D, the simulations performed by Ostriker, Stone, & Gammie (2001) suggest that the stability criterion will still be dominated by the mass-to-flux ratio.

In some of our models, artificial numerical diffusion has turned an initially uniform mass-to-flux ratio λ into a non-uniform distribution, sometimes with striking effects on the numerical stability. While this has a numerical origin, non-uniform distributions of mass-to-flux are also expected on astrophysical grounds. For instance, turbulence provides structures and shocks with small lengthscales and strong magnetic gradients, conditions favorable to a localized, efficient ambipolar diffusion, which can redistribute mass and magnetic flux independently. Cloud collisions can also merge together portions of gas having different masses and magnetic fields. We plan to study directly the physical effect of a non-uniform mass-to-flux ratio in our future work.

This work was supported by NASA grant NAG 5-9180. We thank Jon McKinney, Eve Ostriker, Zhi-Yun Li, and Chris Matzner for comments.

REFERENCES

- Arons, J., & Max, C. E. 1975, *ApJ*, 196, L77
 Basu, S. 2000, *ApJ*, 540, L103
 Chandrasekhar, S., & Fermi, E. 1953, *ApJ*, 118, 113
 Ciolek, G. E., & Mouschovias, T. Ch. 1995, *ApJ*, 454, 194
 Crutcher, R. M. 2004, in *The Magnetized Interstellar Medium*, eds. B. Uyaniker, W. Reich & R. Wielebinski, (Copernicus GmbH: Katlenburg-Lindau), 123
 Drainie, B. T., Roberge, W. G., & Dalgarno, A. 1983, *ApJ*, 264, 485
 Elmegreen, B. G., & Elmegreen, D. M. 1978, *ApJ*, 220, 1051
 Evans, C. R., & Hawley, J. F. 1988, *ApJ*, 332, 659
 Frigo, M., & Johnson, S. G. 2005, *Proc. IEEE*, 93, 216
 Gammie, C. F., Lin, Y.-T., Stone, J. M., & Ostriker, E. C. 2003, *ApJ*, 592, 203
 Gammie, C. F., & Ostriker, E. C. 1996, *ApJ*, 466, 814
 Goldreich, P., & Kwan, J. 1974, *ApJ*, 189, 441
 Goldstein, M. L. 1978, *ApJ*, 219, 700
 Goodman, A. A., Bastien, P., Myers, P. C., & Ménard, F. 1990, *ApJ*, 359, 363
 Hawley, J. F., & Stone, J. M. 1995, *Comput. Phys. Commun.*, 89, 127
 Kulsrud, R., & Pearce, W. P. 1969, *ApJ*, 156, 445
 Ledoux, P. 1951, *Ann. d'Astrophys.* 14, 438
 Mac Low, M.-M., Klessen, R. S., Burkert, A., & Smith, M. D. 1998, *Phys. Rev. Lett.*, 80, 2754
 Mac Low, M.-M., & Klessen, R. S., 2004 *Rev. Mod. Phys.*, 76, 125

- McKee, C. F. 1989, *ApJ*, 345, 782
 Mestel, L., & Spitzer, L., Jr. 1956, *MNRAS*, 116, 503
 Nakano, T., & Nakamura, T. 1978, *PASJ*, 30, 671
 Nakano, T. 1988, *PASJ*, 40, 593
 Ostriker, E. C., Gammie, C. F., & Stone, J. M. 1999, *ApJ*, 513, 259
 Ostriker, E. C., Stone, J. M., & Gammie, C. F. 2001, *ApJ*, 546, 980
 Sagdeev, R. Z., & Galeev, A. A. 1969, *Nonlinear Plasma Theory* (New York: W. A. Benjamin)
 Shu, F. H., Adams, F. C., & Lizano, S. 1987, *ARA&A*, 25, 23
- Spitzer, L., Jr. 1942, *ApJ*, 95, 329
 Stone, J. M., & Norman, M. L. 1992, *ApJS*, 80, 753
 Stone, J. M., & Norman, M. L. 1992, *ApJS*, 80, 791
 Stone, J. M., Ostriker, E. C., & Gammie, C. F. 1998, *ApJ*, 508, L99
 Truelove, J. K., Klein, R. I., McKee, C. F., Holliman, J. H., II, Howell, L. H., & Greenough, J. A. 1997, *ApJ*, 489, L179
 Zuckerman, B., & Palmer, P. 1974, *ARA&A*, 12, 279

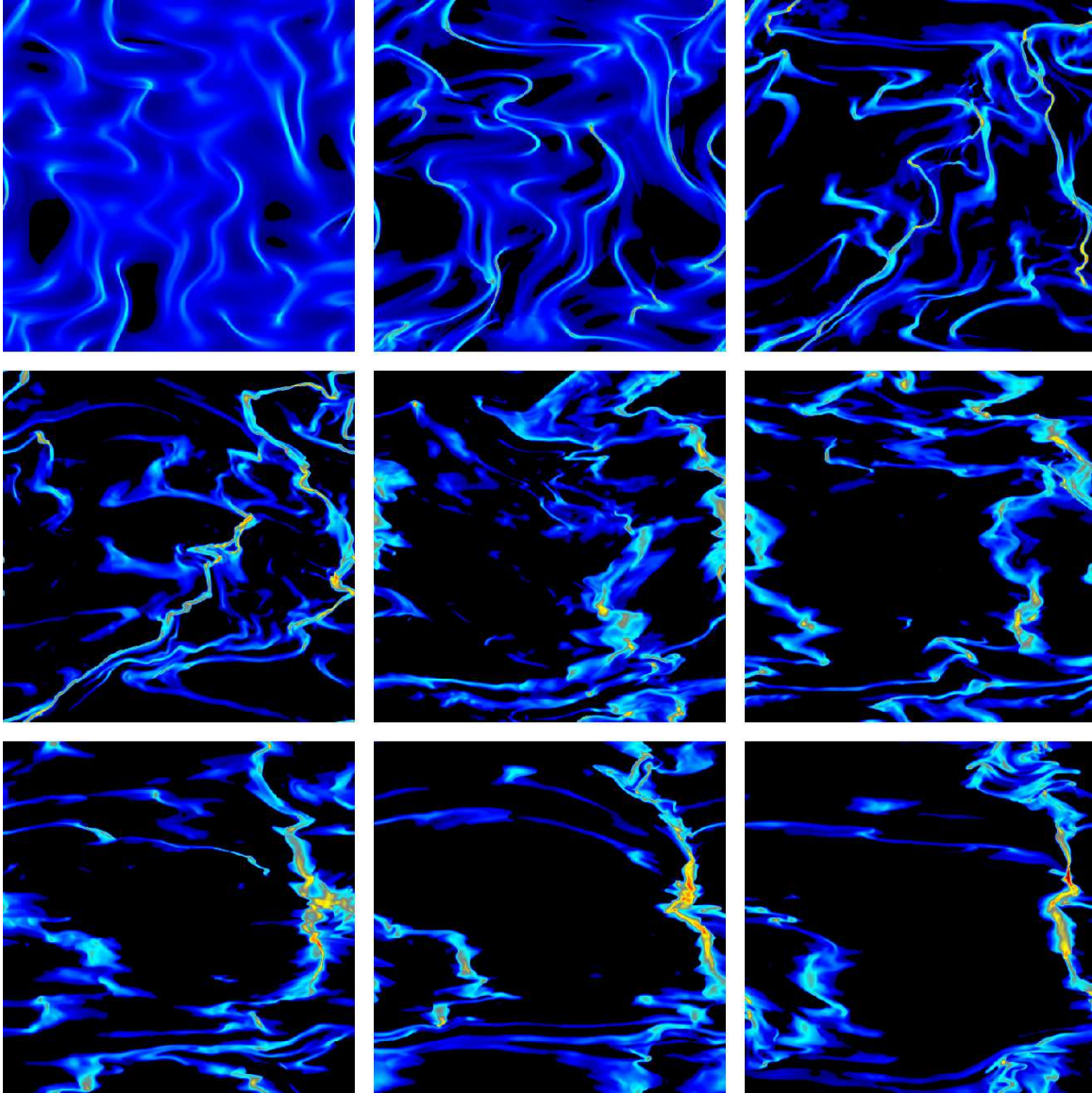


FIG. 1.— Colormaps of ρ in the fiducial run. Snapshots at times $t = 0.01, 0.02, 0.04, 0.06, 0.12, 0.18, 0.24, 0.30,$ and 0.34 . The logarithmic colorscale goes from dark blue (saturating on black) to deep red, corresponding to densities going from $0.01\rho_S = 0.4441\bar{\rho}$ to $10\rho_S = 444.1\bar{\rho}$, where ρ_S is the peak density of an equilibrium Spitzer sheet for the given parameters.

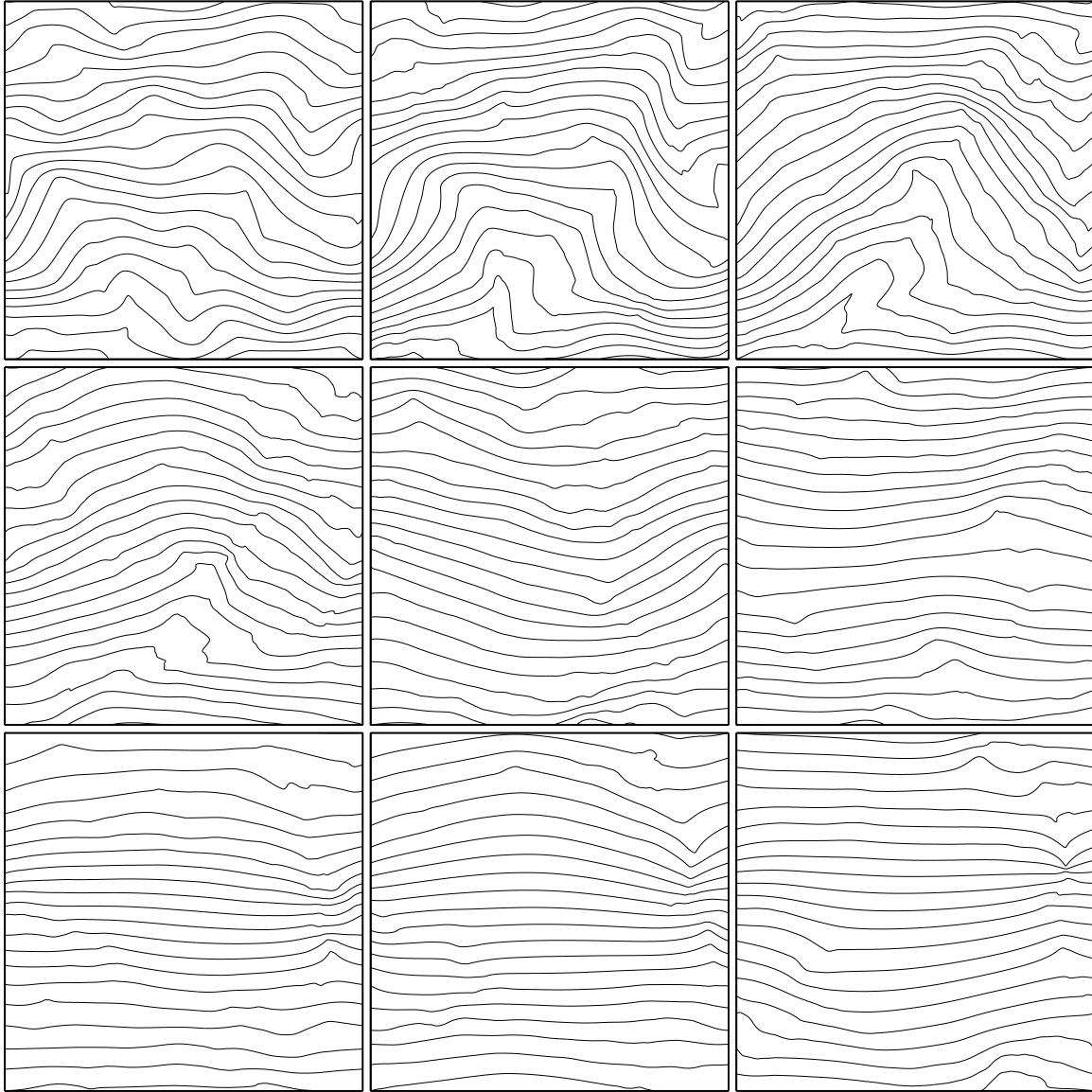


FIG. 2.— Field lines in the fiducial run. The figure shows snapshots at times $t = 0.01, 0.02, 0.04, 0.06, 0.12, 0.18, 0.24, 0.30,$ and 0.34 .

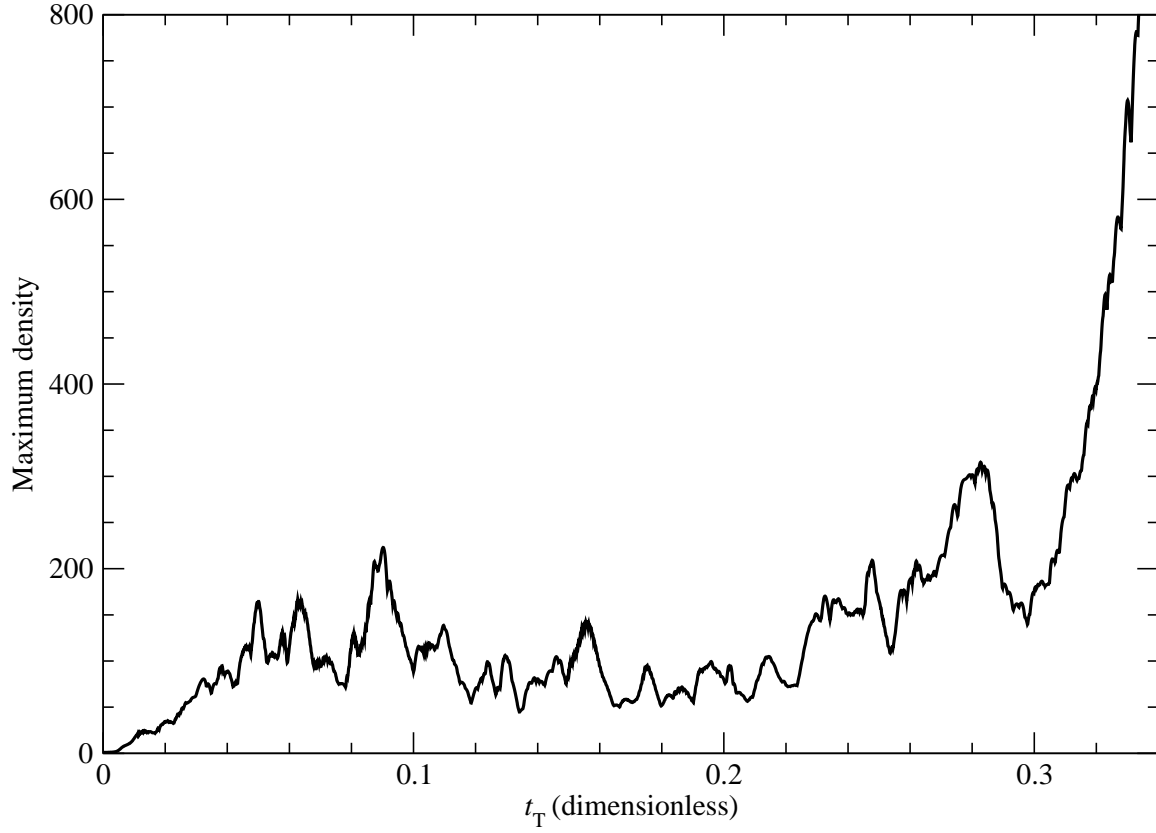


FIG. 3.— Increase of the maximum mass density ρ_{\max} with time in the fiducial run. The run finishes when $\rho_{\max} = 1820$, the Truelove value, at a time $t = 0.341$, slightly beyond the plotted region. Some of the transient peaks shown here could have provoked a numerical instability at a resolution smaller than the value $N = 512$ adopted for the fiducial run.

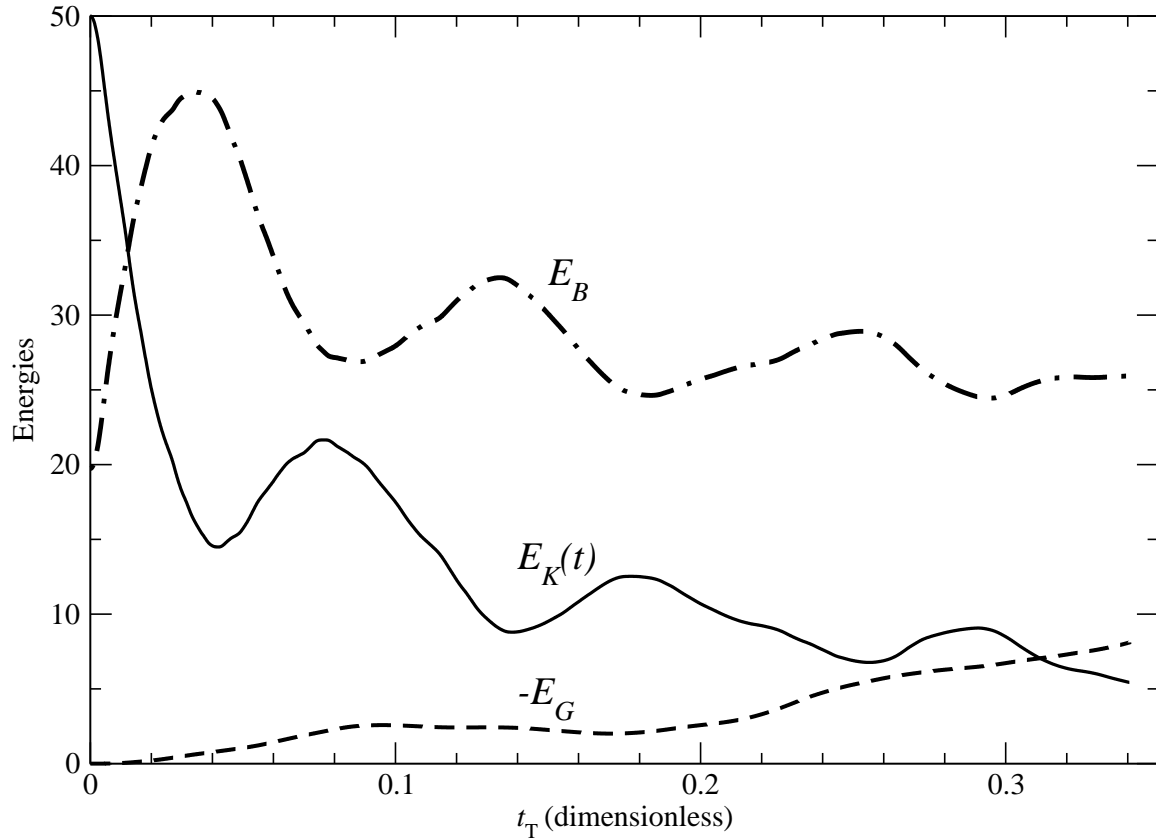


FIG. 4.— Variations in time of the turbulent kinetic energy E_K , the total magnetic energy E_B , and (minus) the gravitational energy $-E_G$.

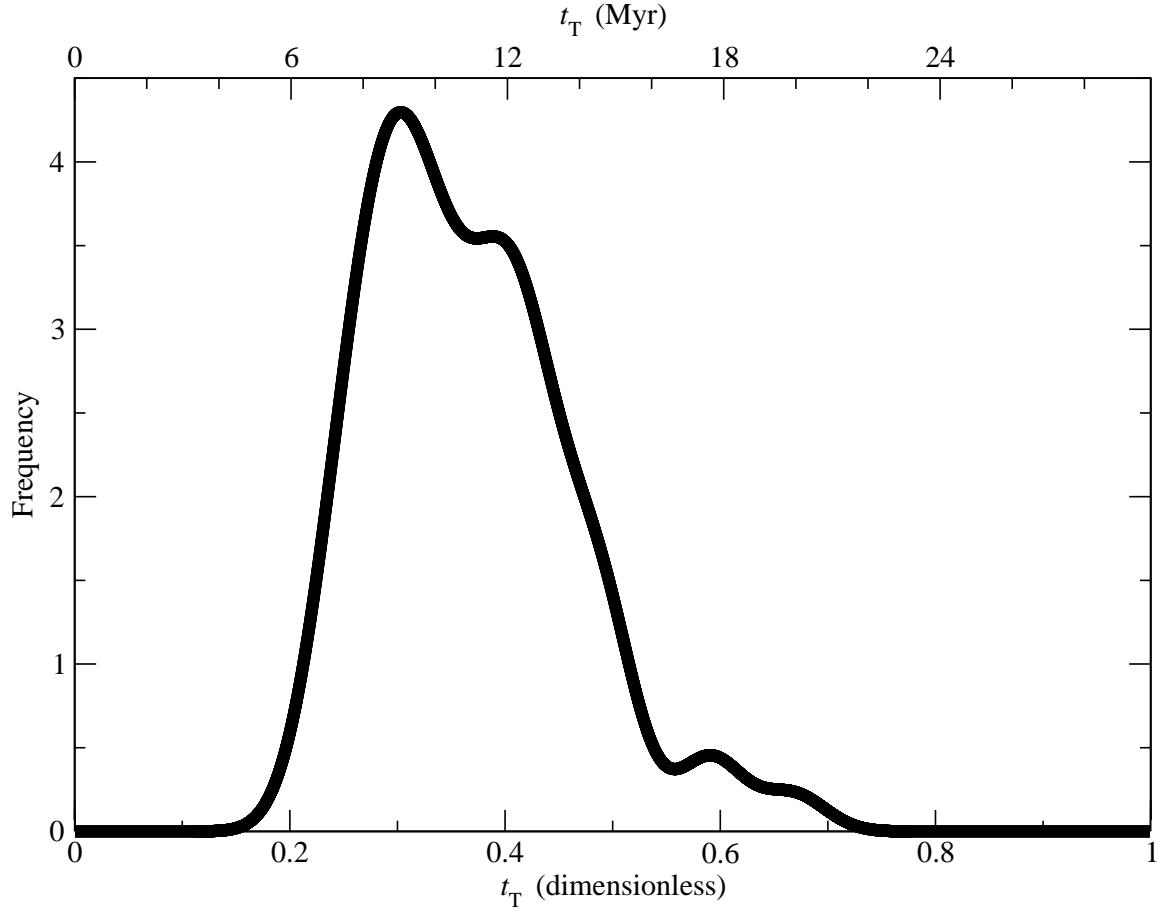


FIG. 5.— Frequency of the different values of t_T . Sixty simulations have been run with the parameters $\lambda = 1.5$, $E_K = 50$, $N = 512$, and different random seeds. Each of these runs has reported a value of t_T . This plot was constructed by summing 60 Gaussian profiles (with $\sigma = 0.03t_s = 0.9\text{Myr}$) centered at each of these t_T values. Collapse times range from ~ 7 to 20Myr .